Crystallization and Separation of Potassium-Containing Salts in Sodium Aluminate Solution

Jilong Liu[1], Xiaolin Pan[2] and Haiyan Yu[3]
1. Distinguished Associate Researcher
2, 3. Professors
Northeastern University - School of Metallurgy, Shenyang, China
Corresponding author: panxl@smm.neu.edu.cn
https://doi.org/10.71659/icsoba2025-aa012

Abstract

The dissolution of potassium-containing minerals in bauxite leads to a large amount of potassium ions entering the sodium aluminate solution, which severely affects the seed precipitation rate of the sodium aluminate solution, as well as the crystal morphology, particle size, and quality of the precipitated products. To achieve the economical and efficient removal of potassium ions from sodium aluminate solution, a single-stage double salt crystallization (SDSC) process is proposed, using Na_2SO_4 as an additive to remove potassium in the form of the double salt $3K_2SO_4{\cdot}Na_2SO_4{\cdot}9H_2O$. The potassium removal performance and mechanisms under different crystallization regimes and solution compositions are systematically studied. The results show that increasing the amount of additive and reaction temperature promotes the crystallization of the $3K_2SO_4{\cdot}Na_2SO_4{\cdot}9H_2O_3$ double salt, thereby improving the potassium removal rate. However, the increase in caustic soda concentration leads to an increase in the number of chain polymers and ion pairs in the solution, hindering solute diffusion, which significantly reduces the potassium removal rate. Under optimal conditions, the potassium removal rate from the sodium aluminate solution can reach 85.68 %, with the potassium concentration dropping from 120 to 24.54 g/L. Additionally, molecular dynamics simulation results indicate that carbonate and oxalate in the sodium aluminate solution exhibit strong interactions with the (0 0 1) face of $3K_2SO_4{\cdot}Na_2SO_4{\cdot}9H_2O$, and their adsorption on the crystal face inhibits crystal growth.

Keywords: Sodium aluminate solution, Alumina, Potassium ions, Double salt crystallization, Molecular dynamics simulation.

1. Introduction

The Bayer process is an industrial chemical process widely used for producing alumina from bauxite [1, 2]. During the Bayer process, impurities such as silicates, organic compounds, and inorganic salts from bauxite and additives are dissolved in the alkaline solution, thus entering the sodium aluminate solution, and gradually accumulate during the recycling process [3, 4]. The concentrated impurities not only increase caustic soda loss but also raise the viscosity of the solution [5]. Furthermore, inorganic anions and impurities such as oxalates can co-precipitate with aluminium hydroxide, leading to a decrease in the quality of the final alumina product [6, 7]. Researchers have conducted extensive studies on the removal of impurities like silica, titanium, iron, vanadium, and organic compounds from sodium aluminate solution, developing various impurity removal techniques such as precipitation, electrochemical methods, solvent extraction, and ion exchange [8, 9]. However, there has been limited focus on the removal of potassium from sodium aluminate solution, and corresponding technological developments are still in their early stages.

Potassium in bauxite primarily exists in minerals such as illite ($K_{0.75}(Al_{1.75}R)(Si_{3.5}Al_{0.5}O_{10})(OH)_2$), potassium feldspar, mica, and others. During the digestion process, potassium enters the sodium aluminate solution and concentrates as the solution undergoes repeated cycles. Although a small

amount of potassium may enter bauxite residue and be discharged with it, most potassium remains in the solution. When using potassium-rich bauxite, the potassium concentration in industrial sodium aluminate solution can reach 100–120 g/L. The presence of potassium reduces the nucleation rate of aluminium hydroxide and prolongs the induction period of seed crystals during precipitation [10]. Therefore, the growth rate of aluminium hydroxide crystals in potassium aluminate solution is significantly slower than in sodium aluminate solution [11]. Moreover, the high potassium concentration during seed crystal precipitation can easily trigger secondary nucleation, leading to the formation of numerous small particles, which impacts the precipitation process and product quality. Consequently, controlling the potassium ion concentration at a lower level during alumina production is crucial for improving both alumina yield and quality.

Due to the similar chemical properties of potassium and sodium, separating them in an alkaline solution is challenging. Xue et al. [12] developed a solvent extraction method to treat potassium aluminate solution, using alkylphenols as extractants, followed by back-extraction for potassium recovery; however, this method could only remove about 40% of the potassium. Crystallization is a commonly used technique for solution purification and is widely applied in separating salts with similar chemical properties. Studies show that potassium can be recovered as potassium carbonate from Bayer spent liquor through multi-stage vacuum evaporation and cooling crystallization processes [13]. Ma et al. [14] extracted potassium nitrate from Bayer spent liquor through multi-stage recrystallization. However, the crystallization processes mentioned above are complex, energy-intensive, slow in reaction rate, and require several days for the separation process.

Therefore, this study proposes an energy-efficient single-stage double salt crystallization (SDSC) process, using Na_2SO_4 as an additive to remove potassium from sodium aluminate solution in the form of the double salt ($3K_2SO_4 \cdot Na_2SO_4 \cdot 9H_2O$). The impact of various reaction conditions on potassium removal is systematically investigated, and the micro-morphology and phase composition of the crystallization products are analysed. Additionally, molecular dynamics simulations are used to explore the mechanism by which impurity ions affect the crystallization process. This research provides a theoretical and technical foundation for the efficient removal of potassium in the Bayer process.

2. Experimental Methods

2.1 Preparation of Sodium Aluminate Solution

The chemicals used in the experiment included sodium aluminate, sodium hydroxide, potassium hydroxide, and sodium sulphate (analytical grade, Tianjin Kemiou Chemical Reagent Co., Ltd.). These chemicals were mixed in specific proportions and dissolved under heating. After filtration, a potassium-containing sodium aluminate solution was obtained. The concentrations of alumina and caustic soda in the sodium aluminate solution were determined by EDTA (ethylenediaminetetraacetic acid) complexometric titration and acid-base titration, respectively.

2.2 Crystallization Removal of Potassium

Potassium removal experiments were conducted using sodium sulphate as an additive. Solid sodium sulphate was added to the potassium-containing sodium aluminate solution. After stirring and dissolution, the solution was placed in a constant-temperature water bath at 90 °C and evaporated for 60 minutes to reach a supersaturated state. The solution was then maintained at various temperatures to promote crystallization, with the stirring speed held constant at 60 rpm during the crystallization process. The crystallization temperature T was set between 50–90 °C, crystallization time *t* ranged from 10 to 120 minutes, the initial potassium concentration was 40–120 g/L, and the caustic soda concentration in the sodium aluminate solution was 100–350 g/L.

Based on stoichiometric ratios, the additive dosage (*S/K*, molar ratio of Na_2SO_4 to KOH) was examined at levels of 1.0, 1.3, 1.6, 2.0, and 2.4. After the reaction, the mixture was centrifuged in a high-speed centrifuge for 3 minutes. Potassium ion concentration was measured using an atomic absorption spectrometer (TAS-986, Beijing Purkinje General Instrument Co., Ltd.), and the potassium removal rate η was calculated using Equation (1):

$$\eta = \frac{C_1V_1\text{-}C_2V_2}{C_1V_1} \times 100\ \% \quad (1)$$

Where:
C_1 Potassium ion concentration in the original solution, g/L
V_1 Volume of the original solution, mL
C_2 Potassium ion concentration in the treated solution, g/L
V_2 Volume of the treated solution, mL.

2.3 Product Characterization

XRD (Philips X'Pert PW3040-60X) was used to analyse the phase composition of the digested solid. Instrument parameters included Cu Kα radiation, tube voltage of 40 kV, tube current of 40 mA, scanning speed of 5°/min, and scanning range from 5° to 90°. Scanning electron microscopy (SEM, SHIMADZU SSX-550) was used to analyse the microstructure and morphology of the digested solid, with an operating voltage of 15 kV. An energy-dispersive spectrometer (EDS, DX-4) was used to analyse the elemental composition of the products.

2.4 Molecular Dynamics Simulation

Molecular dynamics simulations and 3D structure visualization of impurity ion adsorption behaviour were performed using the Materials Studio computational software. The impurity ions included aluminate, carbonate, and oxalate. The crystal structures of $NaAl(OH)_4$, Na_2CO_3, and $Na_2C_2O_4$ were obtained from the Cambridge Crystallographic Data Centre (CCDC). The stability of different crystal planes of the $3K_2SO_4{\cdot}Na_2SO_4{\cdot}9H_2O$ crystal was simulated to identify the dominant crystal face during crystallization. First, the (0 0 1) crystal face of $3K_2SO_4{\cdot}Na_2SO_4{\cdot}9H_2O$ was cleaved and extended to construct a 2×7 supercell of the stable surface. A solvent layer was added above the crystal, consisting of 500 H_2O molecules and additive molecules randomly distributed according to a predetermined density. A 50 Å vacuum layer was placed above the solvent layer to reduce the effect of solvent interactions caused by periodic boundary conditions. During the simulation, the COMPASS force field was used, with a time step of 2 fs. System pressure was maintained at 101.325 kPa, and temperature was set to 290 K.

3. Results and Discussion

3.1 Effect of Reaction Conditions on Potassium Removal

The effects of different reaction conditions on potassium removal are shown in Figure 1. With the increase in additive dosage, the potassium removal efficiency rose significantly, reaching a maximum of 85.68 % at S/K = 1.6 (Figure 1a). Increasing the amount of Na_2SO_4 enhances the supersaturation of the solution, thereby promoting double salt crystallization. When S/K exceeds 1.6, further increases in dosage have little effect on improving the removal rate. In addition, excessive additives can cause the solution composition to deviate from the crystallization zone, resulting in a decrease in potassium removal efficiency. Therefore, the optimal Na_2SO_4 dosage corresponds to S/K = 1.6.

As the caustic soda concentration increases, the potassium removal rate first rises and then declines, peaking at 85.68 % when the caustic soda concentration reaches 200 g/L (Figure 1b). Sodium aluminate solution with high caustic concentration exhibits higher supersaturation, which favours double salt crystallization [15]. However, when the caustic soda concentration is further increased to 350 g/L, the potassium removal rate drops sharply to around 40 %. This is because under high caustic conditions, the Na^+ concentration in the solution increases rapidly, causing the Na/K molar ratio to deviate from the theoretical ratio required for double salt formation. As a result, the contact probability between K^+ and SO_4^{2-} decreases, suppressing double salt generation and reducing the potassium removal rate. Moreover, high caustic concentrations promote the formation of chain polymers and ion pairs in sodium aluminate solution, which increases viscosity and hinders solute diffusion. Therefore, the optimal caustic soda concentration is 200 g/L.

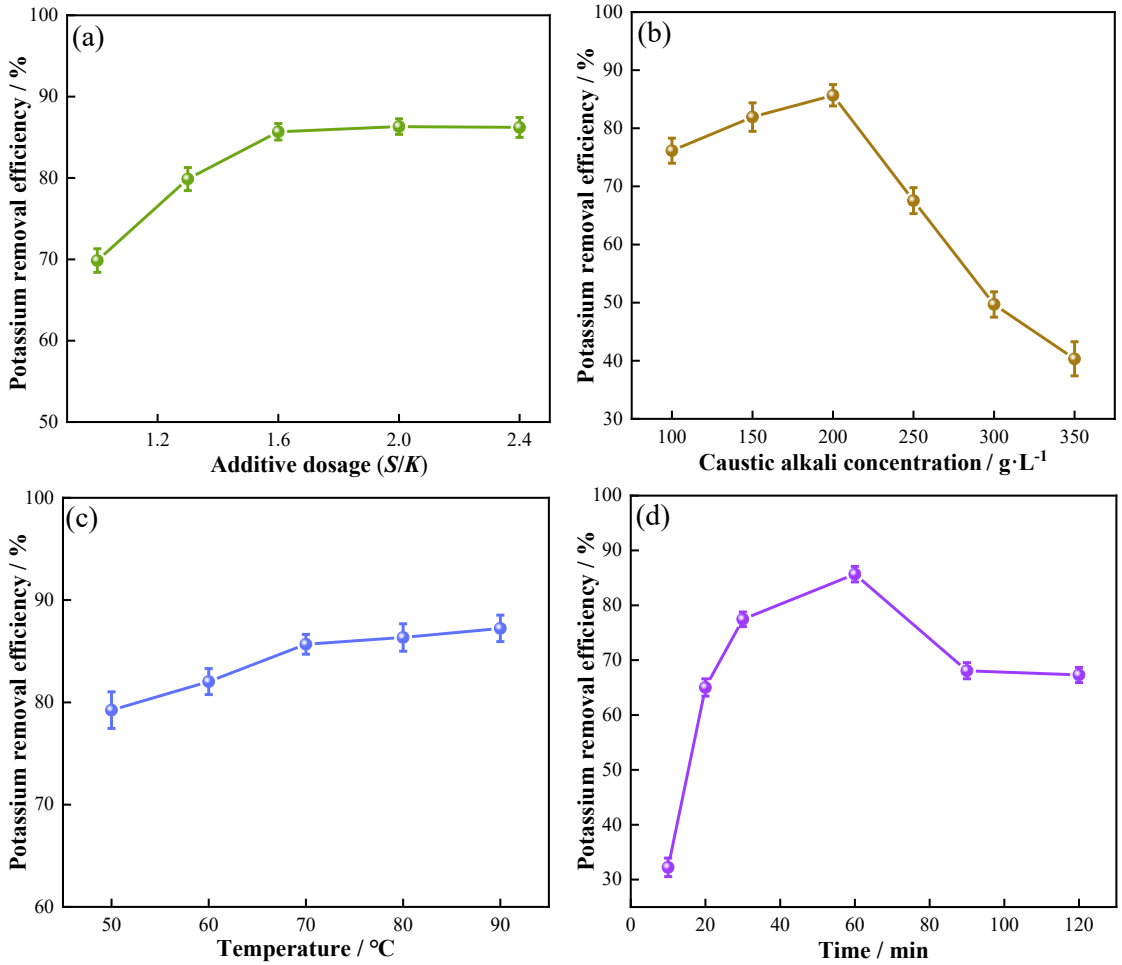

Figure 1. Potassium removal efficiency from sodium aluminate solution under different conditions. (a): additive dosage, (b): caustic alkali concentration, (c): temperature, (d): time.

With the increase in reaction temperature, the potassium removal rate of sodium aluminate solution gradually rises (Figure 1c), indicating that raising the temperature can effectively remove potassium from the solution. Higher temperatures reduce the viscosity of sodium aluminate solution and enhance diffusion, thus shortening the crystallization cycle and facilitating the crystallization reaction. However, because the solubility of the $3K_2SO_4{\cdot}Na_2SO_4{\cdot}9H_2O$ double salt increases with temperature, when the temperature exceeds 70 °C, partial dissolution of the crystallized product occurs, resulting in a slower increase in potassium removal rate.

The potassium removal efficiency increases steadily with reaction time, rising from an initial 32.23 to 85.68 %, an increase of 53.45 percentage points (Figure 1d). Extending the reaction time prolongs continuous crystal growth, thereby promoting the crystallization of $3K_2SO_4 \cdot Na_2SO_4 \cdot 9H_2O$. At the later stage of the reaction, the potassium ion concentration in the solution becomes low, and the driving force for double salt crystallization gradually weakens, leading to a slower growth in potassium removal rate. When the crystallization time exceeds 60 minutes, the potassium removal rate drops rapidly from 85.68 to 68.08 %. This is because prolonged residence time causes partial precipitation of crystallized $3K_2SO_4 \cdot Na_2SO_4 \cdot 9H_2O$ into K_2SO_4 and Na_2SO_4, which re-enter the solution and lower the potassium removal rate. Further extending the crystallization time to 120 minutes shows no significant change, as the $3K_2SO_4 \cdot Na_2SO_4 \cdot 9H_2O$ in the solution has reached dissolution equilibrium. Considering all factors, the optimal crystallization time is 60 minutes.

The optimal conditions for potassium crystallization removal are Na_2SO_4 dosage (S/K) of 1.6, initial caustic soda concentration of 200 g/L, reaction temperature of 70 °C, and crystallization time of 60 minutes, under which the potassium removal rate reaches 85.68 %. The sulphate concentration in the sodium aluminate solution after crystallization remains low at only 0.56 g/L, exerting minimal impact on subsequent production processes.

3.2 Mechanism of Potassium Removal via Crystallization

To investigate the phase composition of the crystallization products, XRD analyses were conducted on products obtained under different conditions, as shown in Figure 2. XRD analysis revealed that when S/K was 1.0, 1.3, and 1.6, the characteristic peak of $3K_2SO_4 \cdot Na_2SO_4 \cdot 9H_2O$ appeared near $2\theta = 31°$, with no other impurity peaks detected. The intensity of the diffraction peak increased with additive dosage (Figure 2a), indicating that the solution composition at these levels was within the crystallization region of $3K_2SO_4 \cdot Na_2SO_4 \cdot 9H_2O$, and the additive amount was appropriate. Further increasing Na_2SO_4 dosage led to the appearance of Na_2SO_4 characteristic peaks, which became stronger as S/K increased. At S/K = 2.4, these peaks dominated the pattern, suggesting an excessive dosage of Na_2SO_4. These results indicate that when S/K is less than 2.0, potassium ions in the sodium aluminate solution can be removed via crystallization of the $3K_2SO_4 \cdot Na_2SO_4 \cdot 9H_2O$ double salt.

XRD results of products under different caustic concentrations are shown in Figure 2b. When the caustic concentration of the sodium aluminate solution exceeded 200 g/L, the intensity of the $3K_2SO_4 \cdot Na_2SO_4 \cdot 9H_2O$ peak at $2\theta = 31°$ gradually decreased, while the Na_2SO_4 peak at $2\theta = 28°$ increased. This indicates that increasing caustic concentration suppressed the crystallization of $3K_2SO_4 \cdot Na_2SO_4 \cdot 9H_2O$, resulting in unreacted Na_2SO_4 being retained in the product. Under different caustic concentrations, the primary phase in the crystallized product remained $3K_2SO_4 \cdot Na_2SO_4 \cdot 9H_2O$, with only a small amount of Na_2SO_4 present.

XRD patterns of products obtained under different crystallization temperatures are shown in Figure 2c. As the temperature increased from 50 to 70 °C, the intensity of the Na_2SO_4 peak at $2\theta = 28°$ gradually decreased and disappeared completely at 70 °C; meanwhile, the intensity of the $3K_2SO_4 \cdot Na_2SO_4 \cdot 9H_2O$ peak at $2\theta = 31°$ tended to increase, reaching its maximum at 70 °C, indicating a better crystallization state. When the temperature was further increased to 90 °C, the peak intensity weakened. This is because at higher temperatures, part of the crystallized $3K_2SO_4 \cdot Na_2SO_4 \cdot 9H_2O$ redissolved, reducing its crystallinity.

When the crystallization time did not exceed 60 minutes, the product contained both $3K_2SO_4 \cdot Na_2SO_4 \cdot 9H_2O$ and Na_2SO_4 phases (Figure 2d). As crystallization time was extended to 60 minutes, the intensity of the Na_2SO_4 peak gradually weakened and eventually disappeared, while the $3K_2SO_4 \cdot Na_2SO_4 \cdot 9H_2O$ peak remained strong, indicating a favourable crystallization

state. During crystallization, after nucleation, crystals require sufficient time to grow into stable forms. Therefore, products obtained in a short time contain a small amount of Na_2SO_4. However, when time was extended to 90 minutes, the Na_2SO_4 peak intensity rapidly increased and became the dominant peak in the XRD pattern. This suggests that with prolonged residence time, $3K_2SO_4{\cdot}Na_2SO_4{\cdot}9H_2O$ crystals redissolve and precipitate into $3K_2SO_4$ and Na_2SO_4, which re-enter the solution. Given the low solubility of Na_2SO_4 in sodium aluminate solution, it precipitates again in abundance, increasing its relative content and gradually transforming the dominant phase in the product to Na_2SO_4.

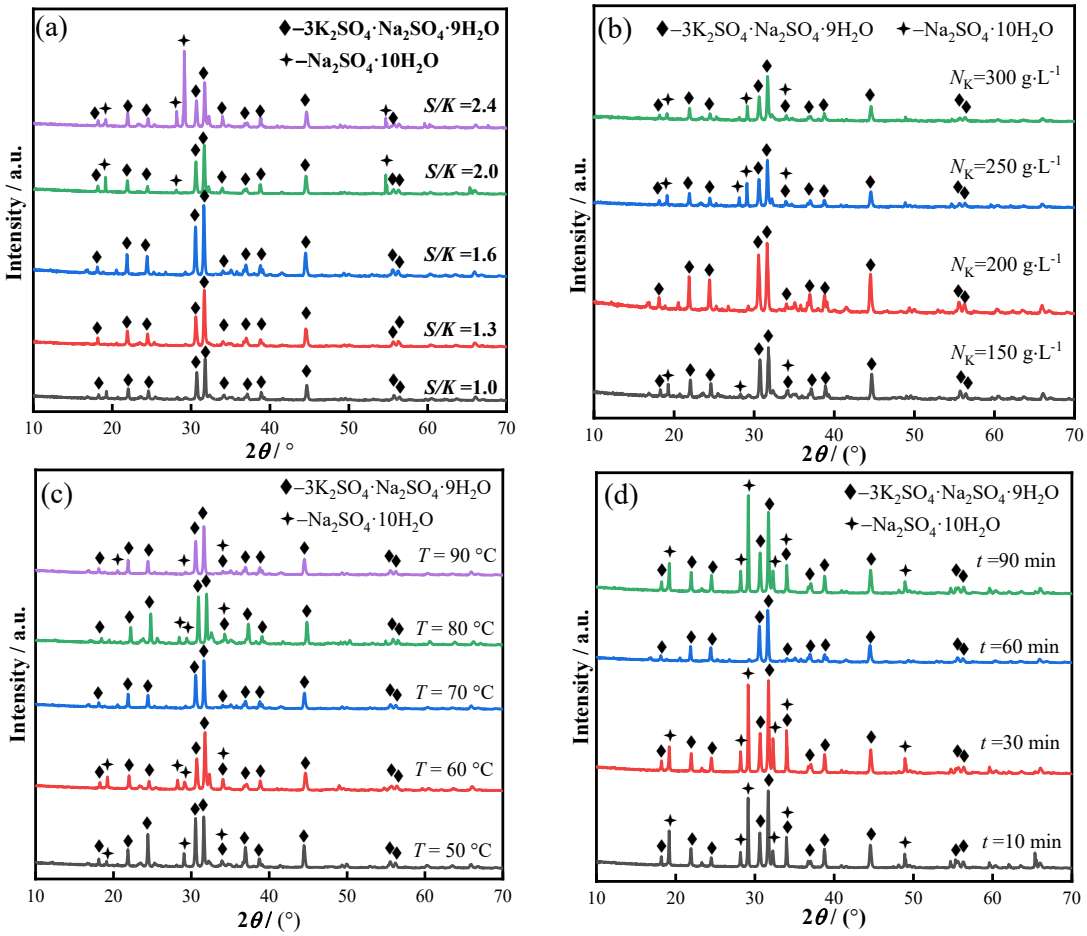

Figure 2. XRD patterns of crystallization products under different conditions. (a): additive dosage, (b): caustic concentration, (c): temperature, (d): time.

The changes in the microstructure of the products during crystallization are shown in Figure 3. At 10 minutes of crystallization, the crystals exhibited an irregular structure and formed clusters that were interconnected (Figure 3b). At 60 minutes, a well-formed crystallized structure was observed (Figure 3c). During crystallization, the crystals displayed different habits, including flaky and prismatic structures (Figure 3d). Most of the prismatic crystals were micron-sized and distributed on the surface of elliptical particles, while the flaky structures were larger in size. When the crystallization time was extended to 90 minutes, the crystal surfaces became rough, showing obvious dissolution (Figure 3f). The elemental composition of the corresponding points in Figure 3 is shown in Table 1. Combining the XRD and EDS results, it can be seen that both the flaky particles (Point A) and prismatic particles (Point B) are $3K_2SO_4{\cdot}Na_2SO_4{\cdot}9H_2O$ double salts, while the internal elliptical particles (Point C) are Na_2SO_4. The fine particles on the surface of the prismatic crystals (Point E) are K_2SO_4, which are produced from the precipitation of

$3K_2SO_4 \cdot Na_2SO_4 \cdot 9H_2O$. During the crystallization process, Na_2SO_4 is encapsulated by the crystallized $3K_2SO_4 \cdot Na_2SO_4 \cdot 9H_2O$ crystals, leading to the formation of agglomerates.

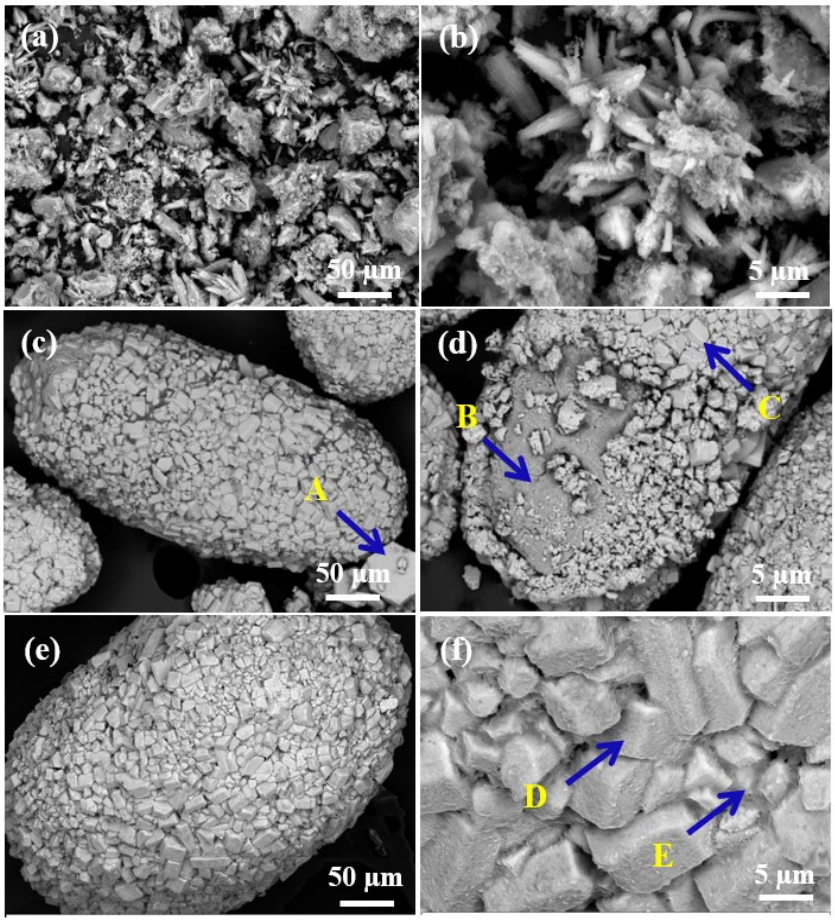

Figure 3. Micro-morphology of crystallization products under different time conditions. (a, b): 10 min, (c, d): 60 min, (e, f): 90 min.

Table 1. EDS Spectral Analysis Results of Crystallization Products.

Data Point	O	Na	S	K	Al
A	49.76	12.45	15.97	21.82	/
B	56.21	30.27	13.53	/	/
C	51.46	11.18	15.53	21.68	0.15
D	62.16	16.32	9.43	11.41	0.69
E	38.82	7.09	20.67	33.12	0.30

3.3 Molecular Dynamics Simulation of Impurity Ion Adsorption

To investigate the mechanism by which impurity ions affect the potassium crystallization process, molecular dynamics simulations were conducted on the adsorption behaviour of impurity ions. The interaction configurations between impurity ions and the (0 0 1) surface during adsorption and at adsorption equilibrium are shown in Figure 4.

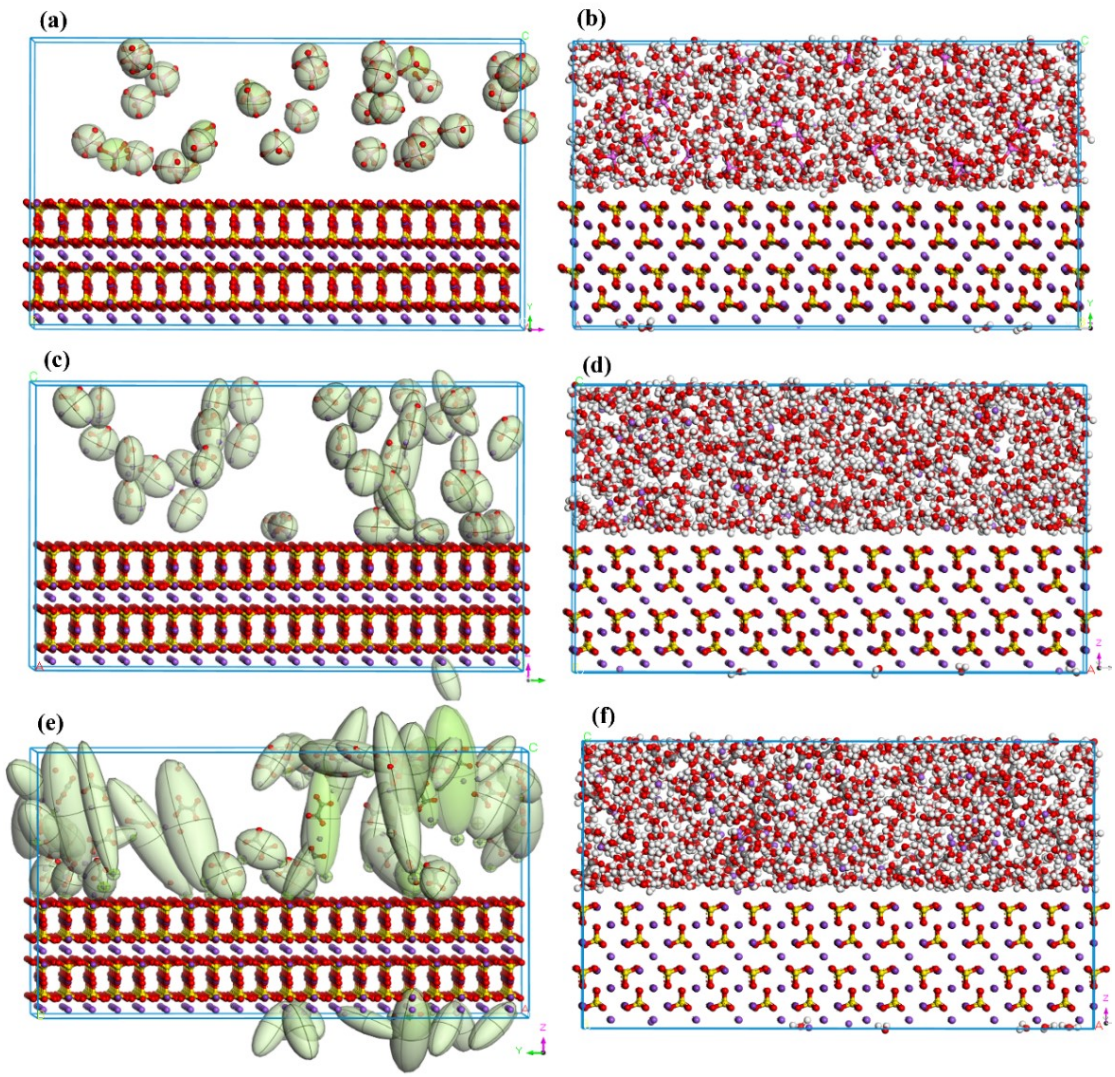

Figure 4. Process models and final configurations of different impurity ions adsorbed on the (0 0 1) surface. (a, b): Al $(OH)_4$; (c, d): CO_3^{2-}; (e, f): $C_2O_4^{2-}$.

At the (0 0 1)-Al $(OH)_4^-$ interface, Al $(OH)_4^-$ forms a molecular layer above the crystal surface, with electronegative groups extending perpendicularly toward the (0 0 1) surface. This is due to the attraction of the positive electrostatic potential around potassium and sodium atoms on the crystal surface. However, because of the relatively low negative charge of Al $(OH)_4^-$, its interaction with the crystal surface is weak, resulting in incomplete adsorption and a limited impact on the crystal growth process. At the (0 0 1)-CO_3^{2-} interface, CO_3^{2-} also forms a layered structure above the crystal surface, but the structure is significantly thicker than that formed in the presence of Al $(OH)_4^-$. Similar to the (0 0 1)-Al $(OH)_4^-$ interface, the electronegative groups of CO_3^{2-} extend perpendicularly toward the (0 0 1) surface. However, unlike the (0 0 1)-Al $(OH)_4^-$ case, some CO_3^{2-} ions are adsorbed onto the crystal surface. This indicates a stronger interaction between CO_3^{2-} and the (0 0 1) surface than with Al $(OH)_4^-$, leading to a greater influence on the crystallization process. This is primarily due to the higher electronegativity of CO_3^{2-}, which makes it more easily adsorbed. $C_2O_4^{2-}$ exhibits the strongest interaction with the (0 0 1) surface; the adsorption configuration shows that most $C_2O_4^{2-}$ ions are adsorbed onto the surface, and the resulting adsorption layer is much thicker than those of Al $(OH)_4^-$ and CO_3^{2-}. Additionally, a small portion of $C_2O_4^{2-}$ migrates through the water layer to the base of the crystal surface, indicating that the electrostatic interaction driving the adsorption has exceeded the repulsive force of the

water molecule layer, allowing $C_2O_4^{2-}$ to penetrate and adsorb onto the crystal surface. Therefore, $C_2O_4^{2-}$ has the most significant impact on crystal growth. For the (0 0 1) surface, impurity anions can be adsorbed and reach adsorption equilibrium within a short period. Due to the higher electronegativity of $C_2O_4^{2-}$ and CO_3^{2-}, their adsorption rates are much faster than that of Al $(OH)_4^-$.

To quantify the interaction forces between impurity ions and the (0 0 1) surface, adsorption energies were calculated, and the results are shown in Table 2. The adsorption energies between the impurity ions and the (0 0 1) surface are all negative, indicating that the surface has a clear adsorption effect on impurity anions. The order of adsorption energy between impurity anions and the (0 0 1) surface is as follows: $C_2O_4^{2-} > CO_3^{2-} >$ Al $(OH)_4^-$. The (0 0 1) surface exhibits the strongest adsorption capacity toward $C_2O_4^{2-}$, with an adsorption energy of -53.86 kJ·mol^{-1}; the weakest is with Al $(OH)_4^-$, with an adsorption energy of only -4.49 kJ·mol^{-1}. The calculated adsorption energies are consistent with the observed adsorption configurations. From an energy perspective, the (0 0 1) surface shows stronger adsorption toward oxalate and carbonate ions, indicating that the adsorption of impurity anions on the crystal surface is related to their charge density and molecular volume. Al $(OH)_4^-$ has a lower charge and is less likely to adsorb onto the (0 0 1) surface, suggesting a minimal inhibitory effect on crystal growth. In contrast, $C_2O_4^{2-}$ and CO_3^{2-} possess higher electronegativity, making them readily adsorb onto the (0 0 1) surface and occupy active growth sites, thereby inhibiting the crystallization of $3K_2SO_4 \cdot Na_2SO_4 \cdot 9H_2O$.

Table 2. Adsorption Energies of Different Impurity Ions on the Crystal Surface

Surface Configuration	E_{Toatl}	$E_{K3Na\ (SO4)2}$	E_{Anion}	Adsorption Energy
(0 0 1)- Al $(OH)_4^-$	-24105.04	-6046.96	-18053.59	-4.49
(0 0 1)- CO_3^{2-}	-21890.61	-6278.06	-15565.19	-43.36
(0 0 1)- $C_2O_4^{2-}$	-20254.86	-6724.31	-13476.69	-53.86

4. Conclusions

1) Increasing the amount of additive and raising the reaction temperature are beneficial for improving potassium removal efficiency. However, at higher caustic concentrations, the efficiency decreases significantly. The optimal process conditions for potassium removal are: additive dosage (S/K) of 2.0, caustic concentration of 200 g/L, reaction temperature of 70 ℃, and reaction time of 60 minutes. Under these conditions, the potassium removal rate from the sodium aluminate solution reaches 85.68 %. The sulphate concentration in the crystallized sodium aluminate solution is relatively low, only 0.56 g/L.

2) The main crystalline phases of the products are $3K_2SO_4 \cdot Na_2SO_4 \cdot 9H_2O$ double salt and Na_2SO_4. The $3K_2SO_4 \cdot Na_2SO_4 \cdot 9H_2O$ double salt exhibits two morphologies: flaky and prismatic, with the flaky crystals being larger in size. As reaction time increases, the $3K_2SO_4 \cdot Na_2SO_4 \cdot 9H_2O$ double salt dissolves, resulting in reduced crystallinity and rougher crystal surfaces.

3) Molecular dynamics simulation results show that impurity ions are adsorbed onto the crystal surface through electrostatic interactions and occupy active growth sites, thereby inhibiting the crystallization of $3K_2SO_4 \cdot Na_2SO_4 \cdot 9H_2O$. The adsorption strength of impurity ions to the crystal surface follows the order: $C_2O_4^{2-} > CO_3^{2-} >$ Al $(OH)_4^-$.

5. References

1. M. Grafe et al., Bauxite residue issues: III. Alkalinity and associated chemistry, *Hydrometallurgy* 108 (2011) 60–79.
2. X.L. Pan et al., Recovery of valuable metals from red mud: A comprehensive review, *Sci. Total Environ*, 904 (2023) 1–18.
3. Y. Lei et al., Leaching behaviors of impurities in metallurgical-grade silicon with hafnium addition, *Hydrometallurgy* 169 (2017) 433–439.
4. H. Peng et al., Aluminate effect on desilication product phase transformation, *J. Cryst. Growth*, 492 (2018) 84–91.
5. G. Power et al., Organic compounds in the processing of lateritic bauxites to alumina part 2: effects of organics in the Bayer process, *Hydrometallurgy* 128 (2012) 125–149.
6. H. Peng et al., The anion effect on zeolite LTA to sodalite phase transformation, *Ind. Eng. Chem. Res.* 57 (31) (2018) 4–24.
7. X.L. Pan et al., Effects of precipitation activity of desilication products (DSPs) on stability of sodium aluminate solution, *Hydrometallurgy* 165 (2016) 261–269.
8. C.D. Zhang et al., Efficient and sustainable process for separating and recovering vanadium from Bayer vanadium sludge using PbSO4 as selective precipitant, *Sep. Purif. Technol* 341 (2024) 126719.
9. Y.B. Zhang et al., Preparation of granular titanium-type lithium-ion sieves and recyclability assessment for lithium recovery from brines with different pH value, *Sep. Purif. Technol* 267 (2021) 118613.
10. J. Li et al., The influence of alkali metal ions on homogeneous nucleation of Al(OH)3 crystals from supersaturated caustic aluminate solutions, *J. Colloid Interface Sci*, 224 (2000) 317–324.
11. L. Zheng et al., Recovery of magnesium and potassium from biotite by sulphuric acid leaching and alkali precipitation with ammonia, *Hydrometallurgy* 157 (2015) 188–193.
12. J. Xue et al., Recovery of potassium hydroxide from strong potassium aluminate solutions using solvent extraction with alkyl phenols, *Hydrometallurgy* 184 (2019) 183–191.
13. Z.L. Yin et al., A method for recovering potassium carbonate from alumina production, China Patent (2016) CN105692658A.
14. H.J. Ma et al., A method for extracting potassium nitrate from circulating mother liquor of alumina production by Bayer process, China Patent (2013) CN103601221A.
15. G.A. Moldoveanu et al., Producing high-grade nickel sulphate with solvent displacement crystallization, JOM 54 (2022) 49–53.